Biomedicine & Pharmacotherapy 142 (2021) 112000

Contents lists available at ScienceDirect

Biomedicine & Pharmacotherapy

journal homepage: www.elsevier.com/locate/biopha

Liposomal paclitaxel induces apoptosis, cell death, inhibition of migration capacity and antitumoral activity in ovarian cancer

Raquel Santos Faria [a], Luiza Ianny de Lima [a], Raphael Severino Bonadio [a], João Paulo Figueiró Longo [a], Marjorie Coimbra Roque [b], João Nunes de Matos Neto [c], Sergio Enrique Moya [d], Mônica Cristina de Oliveira [b], Ricardo Bentes Azevedo [a,*]

[a] Department of Genetics & Morphology, Institute of Biological Sciences, University of Brasília, Brasília, DF 70910-900, Brazil
[b] Department of Pharmaceutical Products, Faculty of Pharmacy, Federal University of Minas Gerais, Av. Antônio Carlos 6627, Belo Horizonte, Minas Gerais 31270-901, Brazil
[c] Cettro - Centro de Câncer de Brasília e Instituto Unity de Ensino e Pesquisa, Edifício de Clínicas - SMH/N Quadra 02, 12° Andar - Asa Norte, Brasília, DF 70710-904, Brasília, DF, Brazil
[d] Soft Matter Nanotechnology Group, CIC biomaGUNE, San Sebastian, Guipúzcoa, Spain

ARTICLE INFO

Keywords:
Ovarian cancer
Peritoneal carcinomatosis
A2780 cell line
Liposomal formulations
Paclitaxel

ABSTRACT

The main goal of this study is to evaluate the efficacy of the paclitaxel (PTX) drug formulated with a liposomal nanosystem (L-PTX) in a peritoneal carcinomatosis derived from ovarian cancer. In vitro cell viability studies with the human ovarian cancer line A2780 showed a 50% decrease in the inhibitory concentration for L-PTX compared to free PTX. A2780 cells treated with the L-PTX formulation demonstrated a reduced capacity to form colonies in comparison to those treated with PTX. Cell death following L-PTX administration hinted at apoptosis, with most cells undergoing initial apoptosis. A2780 cells exhibited an inhibitory migration profile when analyzed by Wound Healing and real-time cell analysis (xCELLigence) methods after L-PTX administration. This inhibition was related to decreased expression of the zinc finger E-box-binding homeobox 1 (ZEB1) and transforming growth factor 2 (TGF-β2) genes. *In vivo* L-PTX administration strongly inhibited tumor cell proliferation in ovarian peritoneal carcinomatosis derived from ovarian cancer, indicating higher antitumor activity than PTX. L-PTX formulation did not show toxicity in the mice model. This study demonstrated that liposomal paclitaxel formulations are less toxic to normal tissues than free paclitaxel and are more effective in inhibiting tumor cell proliferation/migration and inducing ZEB1/TGF-β2 gene expression.

1. Introduction

Epithelial ovarian cancer (EOC) has a high incidence throughout the world and is considered one of the most lethal cancers in women [1,2]. As an asymptomatic disease, about 60% of the patients with EOC are diagnosed at an advanced stage, already facing peritoneal carcinomatosis, with an overall 5-year survival rate of approximately 40% [3,4].

Regarding EOC progression, one of the critical moments is epithelial to mesenchymal transition (EMT) which facilitates cancer cell migration and invasion into other tissues. EMT is characterized by the absence of the epithelial state in an undifferentiated migratory mesenchymal phenotype [5–8]. During EMT, several biological events occur, such as the increased expression of the zinc finger E-box-binding homeobox (ZEB1/2) [9], and the transforming growth factor beta (TGFβ) family [10], which initiates the EMT process. These pathways can activate many genes involved in cell proliferation, differentiation, migration and invasion, in addition to survival and apoptosis [11–14]. Therefore, treatments targeting EMT control may benefit EOC patients.

Due to this complex biological behaviour, advanced EOC treatments typically involve different therapeutic protocols, including cytoreductive surgery and adjuvant chemotherapy, predominantly based on platinum and taxanes compounds. Paclitaxel, one of the taxanes drugs, is an option for treating advanced EOC and peritoneal carcinomatosis [15–17]. Paclitaxel binds to tubulin and promotes the assembly of dysfunctional microtubules, thus preventing microtubule depolymerization and triggering a block in the cell cycle, which in turn results in the death of rapidly proliferating tumor cells [18,19]. Despite its wide clinical use, paclitaxel has some severe adverse side effects, including

* Corresponding author.
E-mail address: razevedo@unb.br (R.B. Azevedo).

https://doi.org/10.1016/j.biopha.2021.112000
Received 21 June 2021; Received in revised form 27 July 2021; Accepted 1 August 2021
Available online 20 August 2021

induced myelosuppression, hypersensitivity reactions, neurotoxicity and cardiotoxicity [20].

To improve the survival rate of patients with advanced EOC, several studies have focused on developing new nanoformulation-based therapeutic approaches [21]. Liposomes have been proposed as a paclitaxel carrier to reduce its adverse effects. Liposomes are nano-sized phospholipid vesicles that afford a significant advantage over conventional chemotherapy as carriers of chemotherapeutic agents [22]. They are used for the controlled delivery of antineoplastic drugs to reduce cancer treatment side effects and increase antitumoral activity. Many studies have shown the advantages of using liposomes applied in ovarian cancer treatment [23–26].

In the present study, we investigated the ability of a liposomal paclitaxel (L-PTX) nanoformulation to inhibit EMT in vitro and the antitumoral and toxicity control of A2780 cells in a nude mouse model.

2. Materials and methods

2.1. Liposomal Nanosystem

The liposomal nanosystem was formulated, characterized and the percentage of encapsulation are described according to Barbosa et al., 2015, and Ferreira et al., 2016 [27,28]. Briefly, the nanosystem was produced using the lipid film hydration method for multilamellar vesicle formation. The liposomes contained the chemotherapeutic agent paclitaxel (PTX) (Quiral Química do Brasil S/A, Juiz De Fora, MG, Brazil).

Liposome stability was evaluated by the dynamic light scattering (DLS) method, using a 90-degree angle Zetasizer Nano (ZS90, Malvern Instruments, USA) Samples were diluted 10-fold, with 100 μL liposomal formulation added to 900 μL HEPES buffer. The data acquired represented the average of 3 readings for each sample, frequency of scattering by scattered light intensity. Morphological analysis of the liposomal system was performed by transmission electron microscopy (TEM). Samples (0.5 mg / mL in distilled water) were pipetted onto a 300-mesh copper grid, fixed, and stained with osmium vapor. After 24 h drying, the material was analyzed with a TEM Jeol® 1011 C (Japan) at 80 kV.

2.2. Cell lines and tumor model

A2780 (BCRJ Code: 0031) human ovarian epithelial cancer was obtained from the Rio de Janeiro Cell Bank, kindly provided by Dr. Sônia Nair Báo from the Laboratory of Electronic Microscopy (Department of Cell Biology, University of Brasilia). Ovarian cancer cells were cultured in cell culture flasks using RPMI 1640 medium supplemented with 10% FBS and 1.2% penicillin-streptomycin. We transformed the A2780 cell line with lentiviral transduction of luciferase and GFP (green fluorescent protein) conjugated (Firefly luciferase + eGFPLentifect™ Lentiviral Particles - GeneCopoeia™) to produce the A2780-luc cell line. A2780-luc cells were used to monitor the migration and proliferation of the cells implanted in BALB/c nude mice. The animal facilities at the Catholic University of Brasília, Brazil provided 12-week-old female BALB/c nude mice, weighing approximately 20 g. Animal experiments were approved and performed in accordance with protocol number 60/2017 approved by the Ethics Committee on the Use of Animals (CEUA – University of Brasília).

2.3. Cell viability test

Cells were seeded at 1×10^4 cells/well in 96-well plates and exposed for 24 h to the free PTX (1% DMSO) or the L-PTX (1.5625 – 50 ng/mL^{-1}). The cells were removed after 24 h and incubated with 0.5 mg/mL MTT in a RPMI 1640 culture medium for 3 h. The media containing MTT solution was then discarded, and 150 μL DMSO added to each well to solubilize formazan crystals formed by the mitochondrial enzymes. Formazan absorbance was then measured at a wavelength of 595 nm using a spectrophotometer (SpectraMax M2, Molecular Devices, USA). Absorbance was used as a cell viability index, with the results expressed as a percentage of viability in relation to the control group. Three independent experiments were performed using 6 different concentrations of paclitaxel from a stock solution. The obtained IC_{50} (L-PTX and free PTX, 19.51 ± 6.1, and 24.69 ± 5.25, respectively) values were used for all subsequent in vitro tests.

2.4. Type of cell death evaluation by flow cytometry

A2780 cells were seeded at 6×10^4 cells/well in 12-well plates. After 24 h, 3 cell groups were prepared, each of them was administered a different solution: 1) L-PTX (19.51 ng/mL^{-1}), 2) PTX (24.69 ng/mL^{-1}), and 3) culture medium only (negative control). After 24 h exposure, cells were trypsinized, washed and resuspended in binding buffer (0.1 M HEPES pH 7.4; 1.4 M NaCl and 25 mM $CaCl_2$). Subsequently, 5 μL Annexin V and 10 μL 7-AAD were added to the cell suspensions, which were then incubated for 5 min at room temperature in the dark. The cells were then analyzed by cytometer (BD FACSVerse™, USA), with 10,000 events counted per sample. Results were analyzed using the FlowJo® v10.0.7 software. The quadrants are: lower left (Q4): viable cells (A-; 7AAD-); lower right (Q3): cells in initial apoptosis (A+; 7AAD-); upper right (Q2): cells in late apoptosis (A+; 7AAD+), and upper left (Q1): necrotic cells (A-; 7AAD+).

2.5. Clonogenic assay

A2780 cells were seeded (1×10^5 per well) in 6-well plates and treated with L-PTX (19.51 ng/mL^{-1}) and PTX (24.69 ng/mL^{-1}) for 24 h to assess the ability of cells to proliferate and form colonies. Surviving cells were deaerated and replated. Each group was counted, and 2×10^3 cells were seeded in 6-well plates with RPMI medium (without FBS). After 5 days, the wells were washed with PBS, colonies fixed with methanol and stained with 0.5% crystal violet. The images of the colonies were photographed under a stereomicroscope Leica EZ4 Stereo (Leica - Germany).

2.6. Wound healing assay

To assess the wound healing ability of L-PTX-treated A2780 cells, 1×10^5 cells/well were plated in 12-well plates and incubated at 37 °C for 24 h. A scratch was then made at the bottom of the wells with the tip of a 20 μL pipette, the cells were treated with: 1) L-PTX (19.51 ng/mL^{-1}), 2) PTX (24.69 ng/mL^{-1}), and 3) culture medium (control), and incubated at 37 °C for 24 h. Following incubation, the treatments were removed and the medium renewed (1% FBS). The cells were maintained for further 24 h. Scratch area images were obtained from each group and analyzed at the 3 timepoints (time 0: when the scratch was made; time 1: 24 h after treatment; and time 3: 24 h after treatment was withdrawn) using a phase-contrast EVOS FL microscope (Invitrogen, Carlsbad, CA, USA). The areas were measured using the ImageJ 1.45 software (National Institutes of Health, Bethesda, USA). The healing percentage was calculated (% of scar = healing area x 100 / initial time area).

2.7. Real-Time Cell Analysis (RTCA) migration assay

RTCA was used to determine the migration of A2780 cells after L-PTX treatment. First, the cells were seeded at 6×10^4 cells/well in 12-well plates. The following treatments were then performed: 1) L-PTX (19.51 ng/mL^{-1}), 2) PTX (24.69 ng/mL^{-1}), and 3) culture medium (control). There was no treatment with free PTX as there was no difference in the previous wound healing test result. After 24 h treatment, the cells were washed with 1X PBS, trypsinized, centrifuged, and counted in a Neubauer chamber. 3×10^4 cells were plated in the upper chamber of a CIM Plate without FBS, and the cells were analyzed for 72 h. The manufacturer's xCELLigence® Real-Time Cell Analysis - CIM Protocol (ACEA Biosciences, Inc.) was followed for this assay, and the

resulting data analyzed using the GraphPad Prism 7.0 software.

2.8. Real-time quantitative reverse transcription PCR (RT-qPCR)

A2780 cells were seeded at 1×10^5 cells/well in 12-well plates. The following treatments were then performed: 1) L-PTX (19.51 ng/mL^{-1}), and 2) culture medium (control). After 24 h treatment, the cells were washed with 1X PBS, trypsinized, centrifuged, resuspended in serum-free medium, and seeded in the upper compartment of a Transwell membrane insert with 8 μm pore size in a 24-well plate (Corning). A medium containing 10% FBS was placed in the lower chamber as an attractant. After 48 h, the cells were collected for RNA extraction. Total RNA was extracted from cells using the illustra RNAspin Mini Kit (GE Healthcare) in accordance with the manufacturer's instructions and quantified using a NanoDrop 2000 spectrophotometer (ThermoFisher Scientific). Messenger RNA (mRNA) integrity was evaluated by electrophoresis in 1% agarose gel stained with 0.5 μg/mL^{-1} ethidium bromide. cDNA molecules were obtained using the High-Capacity RNA-to-cDNA™ Kit (Applied Biosystems, CA, USA), following the manufacturer's instructions. The amplification reactions were performed with the TaqMan™ Fast Advanced Master Mix (Applied Biosystems) in a StepOne™ Real-Time PCR System (Applied Biosystems). The 10 μL amplification reactions were performed on 96-well TaqMan™ Array Plates consisting of 5 μL TaqMan™ Fast Advanced Master Mix, 1 μL cDNA template (Table 1), and 4 μL nuclease-free water. The probes are listed in Table 1. The Amplification program: an initial denaturation step at 95 °C for 20 s followed by 40 cycles at 95 °C for 3 min and 60 °C for 20 s. Relative quantification was achieved by the $2^{-\Delta\Delta Ct}$ method, using the mean values of 4 endogenous controls (18 S, GUSB, ACTB and PGK1). Data were expressed as mean ± SD and analyzed with the GraphPad Prism version 6.0 software. Comparisons were made by ANOVA with the Tukey post hoc test.

2.9. Standardization of the ovarian peritoneal carcinomatosis preclinical model

The animals were divided into 4 groups. All animals received the tumor cell transplantation. Each mouse received an intraperitoneal injection (day 0) of 100 μL PBS containing 1×10^6 A2780-Luc cells. The animals were observed on an IVIS® Lumina XR instrument (days: 1, 7, 14, 21, and 28) for tumor growth analysis and euthanized 7 days apart for macroscopic metastasis visualization.

2.10. The in vivo antitumor effect

This stage of the study involved evaluating the antitumor activity of treatments in animals with peritoneal tumors. Five animals per group were treated intravenously in the tail vain with 100 μL L-PTX or PTX (3.0 mg/kg^{-1}), or no treatment (tumor without treatment group). Four doses of treatment were made at 752 h intervals (Fig. 1). For tumor bioluminescence quantification, images were acquired 7 days apart using an IVIS® Lumina Series III imaging system (PerkinElmer Inc.) following intraperitoneal administration of 100 μL D-luciferin (Sigma) at a concentration of 150 mg/kg, with animals anesthetized using 2% isoflurane under oxygen in the imaging chamber. For A2780-Luc cell bioluminescence images, the open emission filter was adjusted, and 20 images were collected at 60 s of exposure for 20 min. A kinetic luminescence curve was constructed, and the peak of the curve chosen as the bioluminescence value. Data were collected using the Living Image 3.0 software (Caliper Life Sciences Inc., Alameda, CA).

Table 1
Probes used in gene expression analysis by RT-qPCR.

Assay ID	Gene Symbol	Gene Name
Hs00232783_m1	ZEB1	zinc finger E-box binding homeobox 1
Hs00361186_m1	TWIST1	twist family bHLH transcription factor 1
Hs00185584_m1	VIM	vimentin
Hs01062014_m1	NOTCH1	notch 1
Hs00166432_m1	NOTCH3	notch 3
Hs00998133_m1	TGFB1	transforming growth factor-beta 1
Hs00234244_m1	TGFB2	transforming growth factor-beta 2
Hs00950344_m1	SNAI2	snail family transcriptional repressor 2
Hs00966585_m1	LAMA5	laminin subunit alpha 5
Hs00230917_m1	BACH1	BTB domain and CNC homolog 1
Hs00765730_m1	NFKB1	nuclear factor kappa B subunit 1

2.11. Animal and Organ Weight Variation

The animals were weighed weekly, and the data compared between groups. On day 30 post tumor treatment, the animals were euthanized with a lethal intraperitoneal dose of Propofol (60 mg/kg) and the organs collected (heart, lungs, liver, spleen, kidneys and brain). These organs were weighed and finally stored in containers with 10% formalin solution and phosphate buffer (pH 7.0).

2.12. Hematological and biochemical analysis

Blood samples were collected by cardiac puncture and evaluated using a hematimeter (LabTest, Brazil), to verify the changes induced by the treatment. Briefly, 300 μL blood was transferred to an EDTA tube suitable for reading on the equipment. The results were statistically analyzed using the Prism 5.0 software, verifying the mean and standard deviation of each group.

The blood was collected for biochemical analysis in tubes with separator gel to obtain the serum and stored at − 20 °C until the moment of analysis. The serum was analyzed using a Chem Well T automatic analyzer, LabTest, Brazil) to determine the following concentrations: alanine aminotransferase (ALT), aspartate aminotransferase (AST), creatinine K, alkaline phosphatase, LDH, and urea.

2.13. Statistical analysis

The results were analyzed using the GraphPad Prism 7.0 software with a significant difference considered as 5%, $p < 0.05$. One-Way ANOVA tests were used, with the Bonferroni post hoc test; and One-Way ANOVA with Bonferroni post hoc test, and the unpaired T-test.

3. Results

3.1. Liposomal nanosystem characterization

The hydrodynamic diameter of the liposomes was 208 nm as determined by DLS. Liposomes displayed a zeta potential of - 5.18 mV, close to neutrality. Morphological analysis of the TEM images showed that the liposomes are spherical-shaped, monodisperse with a homogeneous morphology and approximately 190 nm in diameter, slightly smaller than observed using the DLS technique. Moreover, it was possible to determine that the liposomes are formed by more than 6 bilayers (Fig. 2). These data were comparable to those obtained in the reports by Barbosa et al., 2015; Ferreira et al., 2016 [27,28].

3.2. Cell viability after treatment with L-PTX and mechanism of cell death

According to the viability test results, the 50% inhibitory concentration (IC_{50}) values were 19.51 ± 6.1 when using L-PTX, and 24.69 ± 5.25 for PTX. The subsequent tests were conducted based on the IC_{50} values determined in this step. A2780 cells were treated for 24 h and labeled with Annexin-V and 7-AAD to analyze the cell death profile induced by L-PTX. The exposure of A2780 cells to L-PTX showed a significant increase ($p < 0.0001$) in the number of Annexin labeled cells (22.1%) compared to the control. Cell death profiles of L-PTX treatment suggested apoptosis since most of the cells were present in an early

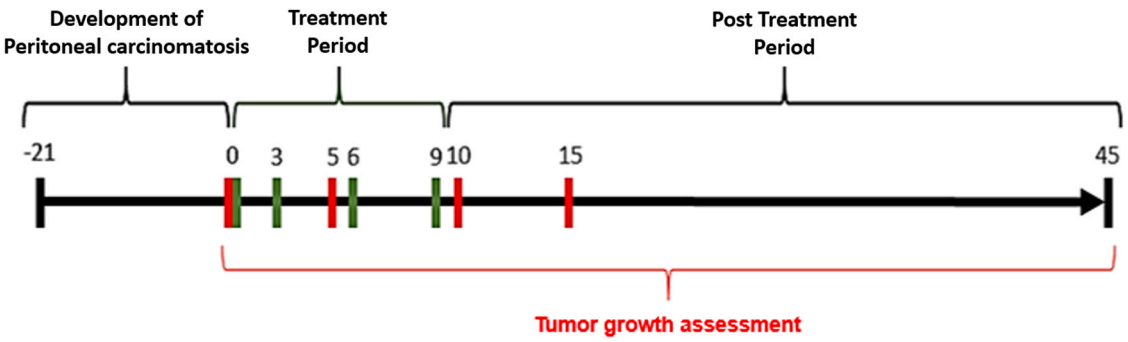

Fig. 1. : Experimental design. Black dividing lines indicate the beginning and end of the experiment; Green lines indicate the days of intravenous treatment; Red lines indicate the days of the analysis.

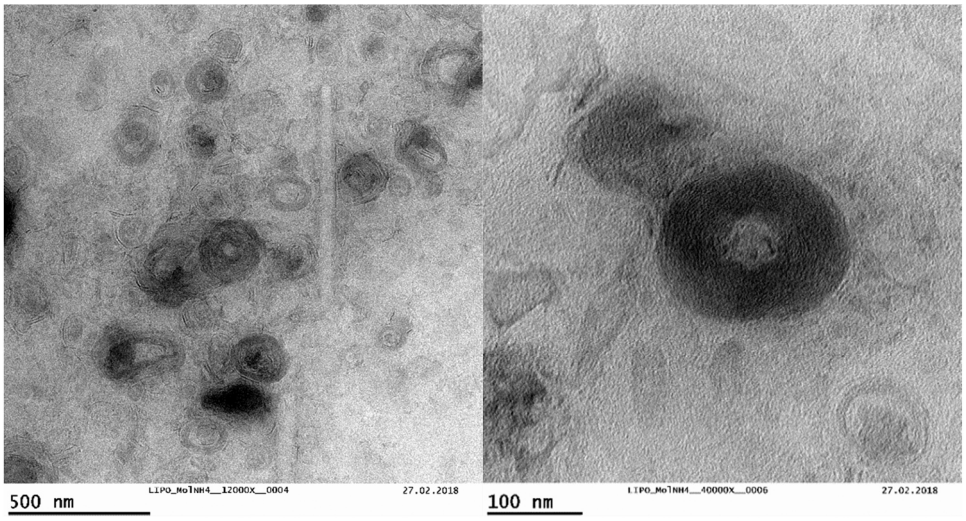

Fig. 2. Transmission Electron Microscopy (TEM) of the liposomes.

apoptosis stage (Fig. 3).

3.3. Clonogenic assay

Fig. 4 shows that untreated cells (negative control) proliferated and formed several colonies of various sizes. Treatment with free PTX obtained a similar pattern to the negative control. It is worth noting that during the treatment with free PTX there was no colony growth. However, colonies started to form after drug removal. The growth rates of the negative control and free PTX-treated colonies were statistically different ($p < 0.001$) from the growth rate of colonies treated with L-PTX.

3.4. L-PTX inhibits cell migration

On analyzing the wound healing assay (two-dimensional assay), it is possible to observe that after 24 h of treatment, the migratory capacity of the untreated group (negative control) was higher than both of the PTX and L-PTX treatment groups ($p < 0.01$) (Fig. 5). The migratory capacity of the negative control group remained higher in the post-treatment evaluation. However, cells treated with free PTX increased their migratory capacity in a similar manner as the negative control group. It was also possible to visualise that the L-PTX treated group inhibited migration, and it was statistically different from the groups treated with free PTX and the negative control (* $p < 0.05$ and ** $p < 0.01$, respectively) (Fig. 5a).

The xCELLigence device recorded the migrating information in A2780 cells for 72 h (three-dimensional assay). The cellular index represented the migratory ability of A2780 cells after treatment with L-PTX and the negative control (Fig. 5b). After treatment with L-PTX, cell migration was reduced compared to the negative control and PTX treatment groups, maintaining the cell index at near 0 throughout the experiment with a significant difference ($p < 0.001$). These results demonstrated that A2780 cells exhibited a migration inhibitory profile following liposomal paclitaxel treatment (L-PTX).

3.5. L-PTX downregulates ZEB1 and TGFB2 expression, altering the migration capability

The expression of migration genes was also evaluated. The data was analyzed using the $2^{-\Delta\Delta Ct}$ method. A p-value ≤ 0.05 was considered statistically significant in the genes. The data are presented as mRNA expression levels in Fig. 6. Considering the results, ZEB1 and TGFB2 were down-regulated ($p < 0.001$), while TGFB1 was up-regulated ($p < 0.05$). All of the other genes studied did not differ from the control.

3.6. Standardization of the tumor model

Bioluminescence studies indicated the presence of tumor cells via the reaction between the luciferase enzyme transfected in the A2780-Luc cells and luciferin, by intraperitoneal injection. Five animals were observed for tumor growth analysis using the IVIS® Lumina XR optical imaging system (days: 1, 7, 14, 21, and 28) and euthanized 7 days apart for macroscopic metastasis visualization. The in vivo analysis on the IVIS Lumina system revealed that the best time to initiate treatment would be 3 weeks post tumor cell inoculation. At this time, we observed

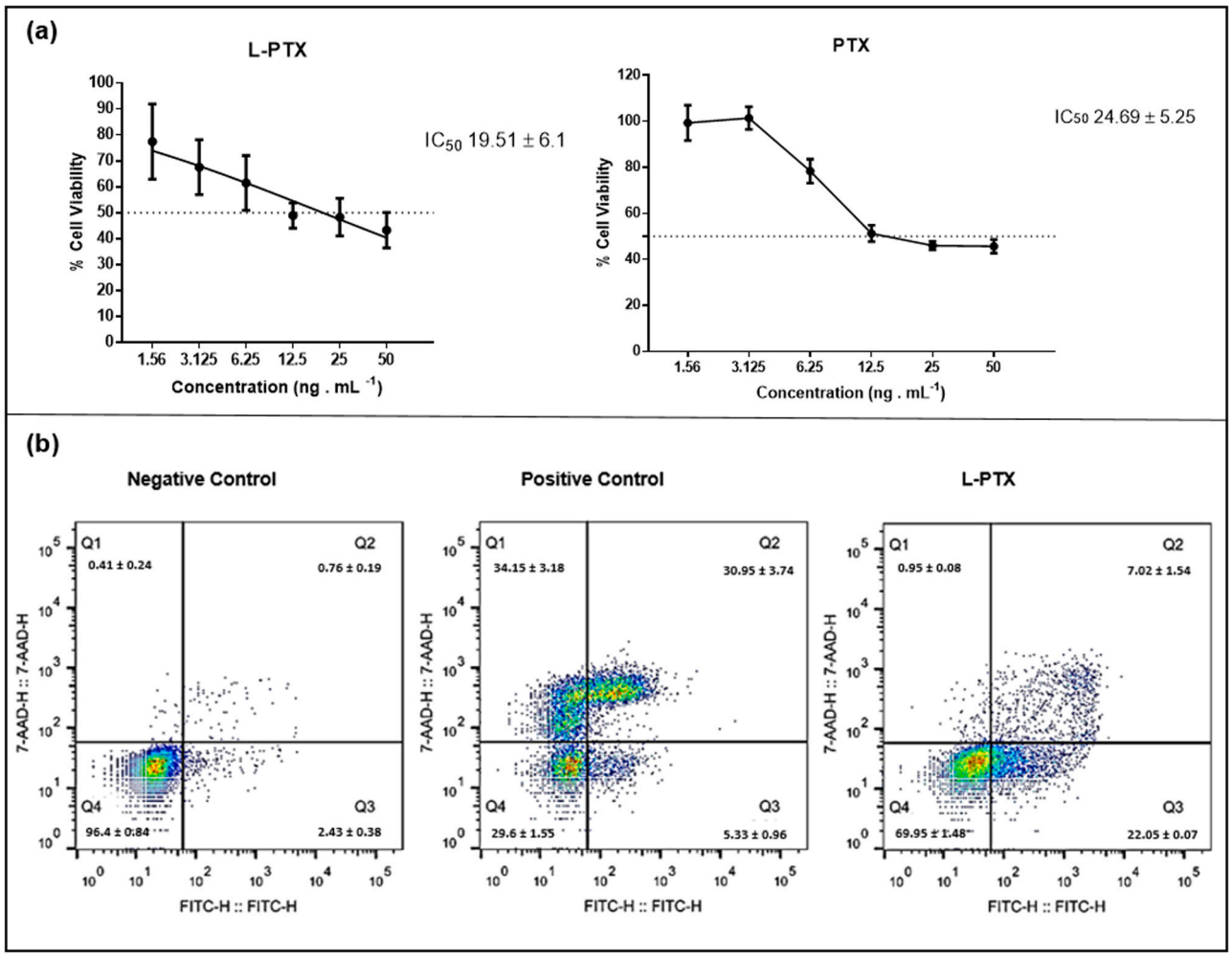

Fig. 3. : (a) IC_{50} values of A2780 cell line treated with free PTX and liposome L-PTX (1.5625 – 50 ng/ mL^{-1}) for 24 hand determined by MTT; (b) Dot plot of the evaluation of cell death type in A2780 ovarian tumor cells after treatment with L-PTX (19.51 ng. mL^{-1}). Cells were labeled with Annexin-V and 7AAD. Data are representative of three independent experiments. Lower left quadrant (Q4): viable cells; lower right quadrant (Q3): early apoptotic cells, upper right quadrant (Q2): late apoptosis cells; upper left quadrant (Q1): necrotic cells.

the presence of the characteristic and delimited metastatic nodules only in the peritoneal region, with no cells present in other organs (Fig. 7).

3.7. Antitumor activity of L-PTX

Bioluminescence radiance analysis was measured 4 times in all 5 animals per group (Fig. 1). No statistical difference in bioluminescence was observed 5 days after treatment initiation (T5). On day 10 post treatment (T10), a statistically significant difference ($p < 0.01$) between the PTX and L-PTX treated groups was observed indicating that animals treated with L-PTX had significantly more tumor growth inhibition than the PTX treated group (Fig. 8).

Analysis on day 15 post-injection (T15), revealed a statistically significant difference between the PTX and L-PTX groups, showing that animals treated with L-PTX had decreased tumor cell proliferation at the end of the evaluation. These results showed that treatment with L-PTX strongly inhibits tumor cell development and proliferation in ovarian peritoneal carcinomatosis, indicating higher antitumor activity than free PTX.

3.8. Reduced Toxicity using L-PTX

The animal's blood count was evaluated at the end of the experiment (Fig. 9a). The total leukocyte counts significantly decreased in animals treated with L-PTX compared to animals with tumors without treatment and free PTX treatment. Moreover, it significantly increased for animals treated with free PTX compared to healthy animals. The same result for free PTX was evaluated for platelet count. There was no statistical difference in red blood cell and hemoglobin counts between the groups.

Loss of body weight can be used to measure drug-induced toxicity. Body weight variation was obtained/ from the animal weight data. Analysis of decreased toxicity by bodyweight variation revealed high antitumor activity when treated with the drug in the liposomal form (Fig. 9b). It is possible to observe a statistical difference regarding animal weights between animals treated with free PTX and animals treated with liposomal PTX ($p < 0.05$). These data indicated that animals treated with L-PTX had weights much closer to healthy animals than those treated with free PTX.

After euthanasia, the relative weight of selected organs (liver, lungs and spleen) was also evaluated (Fig. 9c). A statistically significant difference was observed between the relative liver weight of animals treated with free PTX, Healthy (control?) animals and those treated with L-PTX. A similar observation was made for the relative weight of the lungs from animals treated with free PTX and Healthy animals without treatment (control) and those treated with L-PTX.

The blood was collected for biochemical analysis using a Chem Well T automatic analyzer, (LabTest, Brazil) to determine the following concentrations: alanine aminotransferase (ALT), aspartate

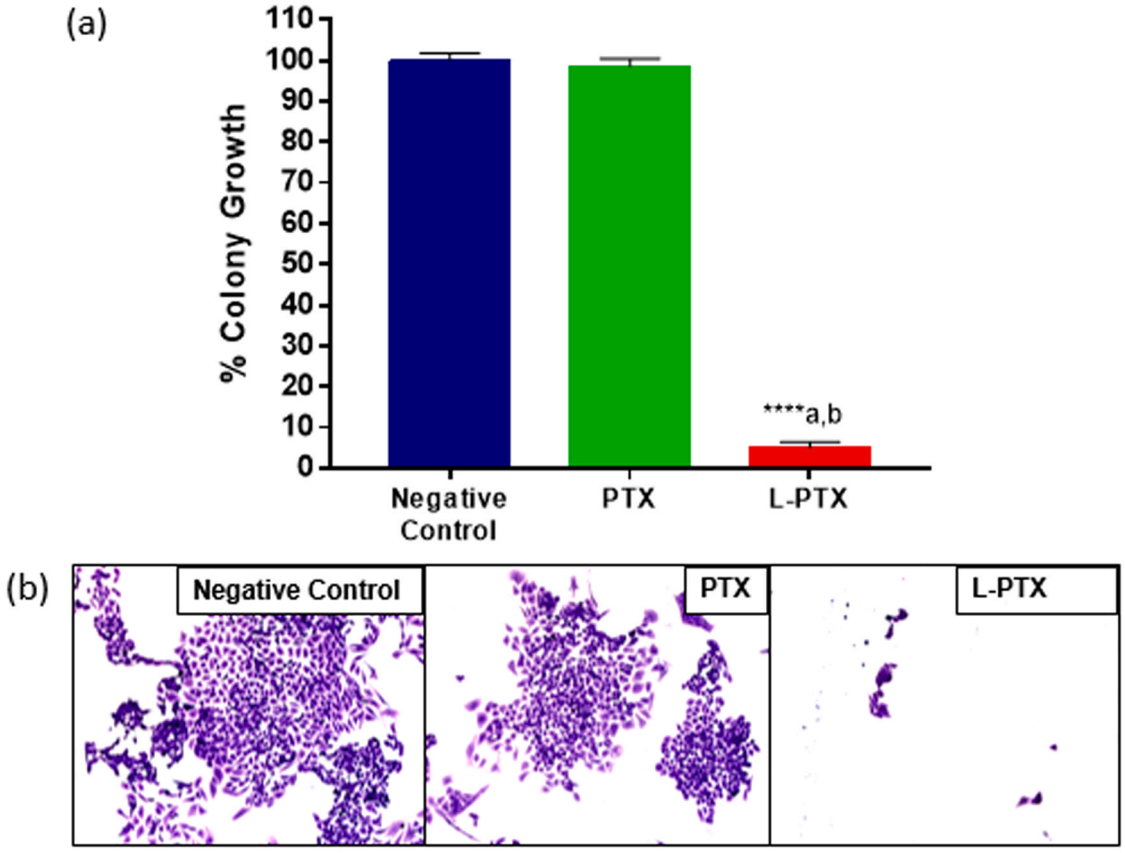

Fig. 4. : Effect of treatment with PTX and liposomes on the colony-forming ability of A2780 cells. A2780 cells were treated with the IC_{50} concentration of free paclitaxel and a liposomal paclitaxel formulation for 24 h, 24.69 and 19.51 ng/mL^{-1}, respectively. After this time, 2000 surviving cells were plated in 6-well plates and cultured for 5 days. (a) Colony growth percentage data of PTX and L-PTX are presented as the mean ± standard deviation of 3 wells in relation to the negative control group (**** $p < 0.001$). (b) Images were obtained under a Leica EZ4 Stereo microscope.

aminotransferase (AST), creatinine K, alkaline phosphatase, LDH, and urea. Our study found no significant difference among the different groups for all variables evaluated.(Fig. 10).

Regarding the leukocyte differentiation parameters described in Table 2, the value referring to the percentage of lymphocytes is low for animals in the PTX treatment group (20.5%), compared with all other groups (61.9%, 45.2%, and 42.7% for healthy, tumor control and L-PTX, respectively), and is statistically different. The percentages of monocytes, basophils, and eosinophils count data showed an increase of the group treated with PTX (68.6%) compared to the other groups: healthy (34.6%), tumor control (50.9%) and L-PTX (53.0%). In the neutrophil value assessment. no statistical difference was observed between the percentages of the different groups.

4. Discussion

This work evaluates antitumoral effects, together with the in vitro and in vivo toxicity, of a liposome encapsulated PTX designed to treat ovarian cancer using an experimental model of metastatic ovarian cancer and peritoneal ovarian carcinomatosis. Results showed that the concentration of liposome encapsulated PTX required to eliminate 50% of the A2780 cells was not statistically different, but it was lower than the free PTX concentration. These results are also correlated with the reduction of cell viability and colony formation in the recovery test for 5 days. After 24 h of treatment, it was observed that the cells treated with L-PTX were unable to proliferate, whereas cells treated with free PTX rapidly returned to initial conditions and formed colonies. The ability of cells to form colonies after treatment with PTX was also shown by Gamarra-Luques and co-workers (2012). The authors demonstrated that in clonogenic assays of OV2008, IGROV-1 and SK-OV-3 cells (ovarian tumor lines) treated with cisplatin and free PTX remained viable after 21 days, and that therapy with PTX, cisplatin or both drugs together, did not decrease cell proliferation. According to the aforementioned authors, cells survival after chemotherapy treatment can be considered a therapeutic failure. In this case, the remaining cells are scarce but still worrying, as is typically the case for patients in the clinic who undergo first-line treatment, as these cells can survive and proliferate, and in many cases with greater capacities than untreated cells [29].

The results of our study (Fig. 4) corroborate those demonstrated by Franco et al. (2019), who evaluated the colony formation capacity and proliferation rate of MCF-7 cells (breast cancer cell line) and reported reduced colony-forming capacity when these cells were previously exposed to L-PTX. In contrast, cells treated with free PTX were able to form colonies [30]. These results indicated that in different cell types, liposomes play a vital role in PTX bioavailability inside the tumor cell, preventing proliferation, that is, without the therapeutic failure that can be observed in treatment with free PTX.

As drug nanocarriers, liposomes can modulate different aspects of drug pharmacokinetics, including molecule dispersion and biological fate, including subcellular distribution. In comparison to free drugs, molecule dispersion is significantly improved when they are entrapped within liposomes. This feature increases drug delivery to cells in vitro, thus increasing the drug effect on cells. Moreover, even though we did not measure subcellular distribution, we have already observed that drugs have different intracellular fates when they are entrapped in nanocarriers [31–33]. Considering that liposomes impact cellular distribution, we can suppose that different cellular components are not equally affected by the different treatments. For instance, a previous

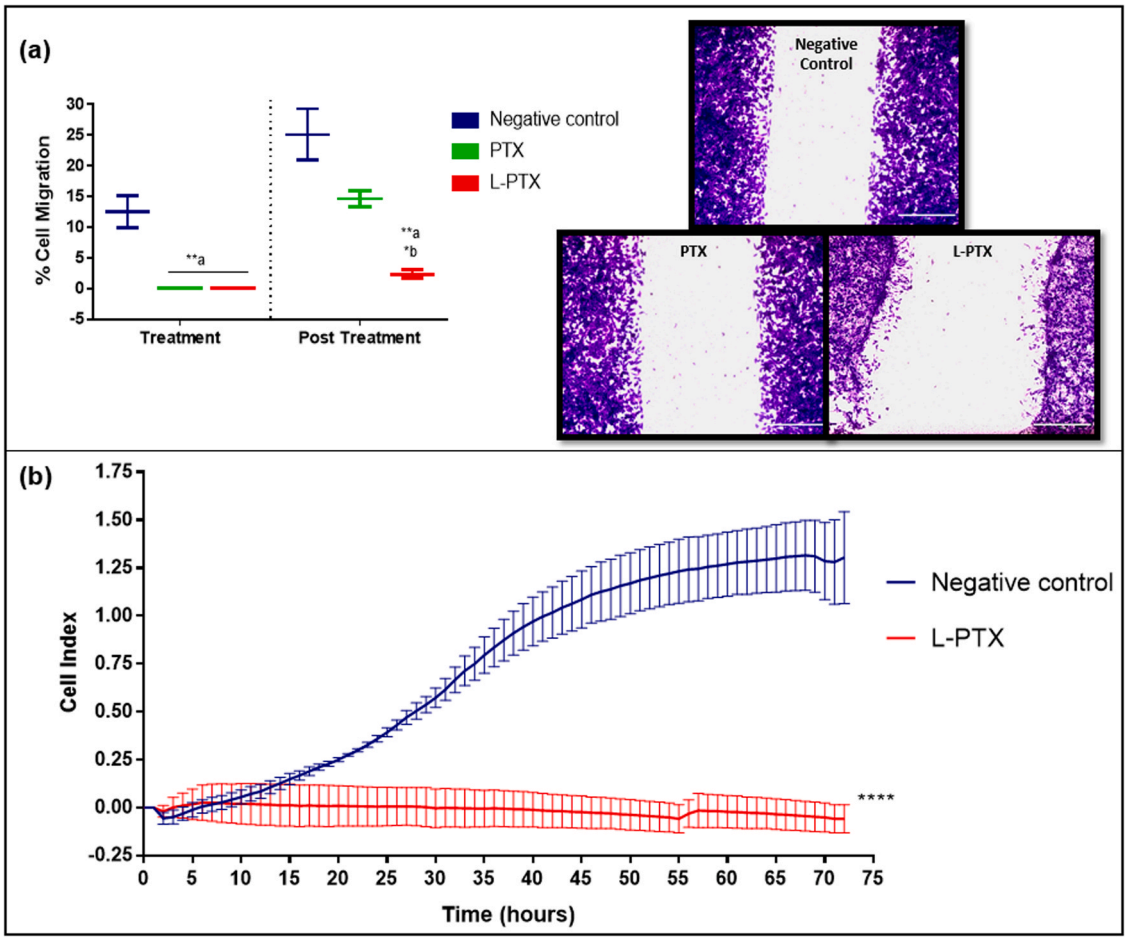

Fig. 5. : (a) The Wound Healing test showed cell migration of A2780 after 24 h of treatment with IC_{50} values of free paclitaxel and liposomal paclitaxel. Data are presented as mean ± standard deviation of 3 wells. (b) The xCELLigence RTCA DP system recorded and collected A2780 cell migration data at 1 h intervals for 72 h following treatment with PTX or L-PTX. Differences in cell indices between the liposome-treated and control groups were significant. Data are presented as the mean ± standard deviation of 3 wells (**** $p < 0.001$).

article [32] reported that doxorubicin can remain in the cytoplasm for longer periods and translocate into the nucleus in a time-dependent manner when entrapped within lipid nanoemulsions. In this situation, structures present in the cytoplasm, such as the cytoskeleton, could be preferentially affected, impacting cell motility and therefore cell invasiveness.

It was also observed in the present study that the L-PTX treatment significantly reduced cell migratory capacity, evaluated for 72 h, indicating that L-PTX was able to inhibit migration of cells of the ovarian lineage during and after treatment, both in the two-dimensional and three-dimensional assays (Fig. 5). It is important to note that in the treatment of A2780 cells with free PTX, it was not possible to observe the continued anti-migratory effect after removing the drug; that is, the cells were able to migrate again.

As previously mentioned, metastasis is the main problem relating to cancer, with 90% of cancer patient deaths caused by metastasis [34]. In epithelial ovarian cancer, metastasis leads to the appearance of peritoneal carcinomatosis which is associated with a poor prognosis in patients [35]. As the migratory capacity of epithelial tumor cells is the initial factor in the occurrence of implantation metastasis [36], we also assessed whether a liposomal PTX system could reverse the migratory capacity of the A2780 cell line. The results of this study corroborate those of Franco et al. (2019) who reported a significant reduction in the percentage of cell migration of MDA-MB-213 and MCF-7 cells (breast tumor lines) treated with L-PTX when compared to the control group [37]. These results provide strong evidence of the importance of the liposomal nanocarrier in the cells' PTX role/role of PTX in cells.

The acquisition of the migration ability by epithelial cells involves changing morphology to a fibroblastoid format, indicating a loss of expressing epithelial markers and a gain of expressing mesenchymal markers. This phenotypic conversion is one of the events allowing epithelial cells to migrate from primary tumors and form metastases in distant tissues or organs. One of the molecular mechanisms involved in this process includes signaling pathways mediated by members of the TGF-β family [38–41]. Taking this into consideration, we evaluated the expression of molecules involved in EMT via TGF-β activated cytoplasmic signaling. The results showed that treatment with L-PTX decreases TGF-β2 and ZEB1 gene expression and increases TGF-β1 expression (Fig. 6).

Based on these data, we believe that the inhibition of cell migration after treatment with L-PTX observed in this study may be related to decreased expression of the TGF-β2 and ZEB1 genes. This modification in the expression of TGF-β in the development and metastasis of cancer is similar to the physiological signaling during embryonic development, in which EMT (epithelium-mesenchymal transition) generates and forms new tissues [42,43]. This pathway participates in the pathogenesis of many types of cancer, contributing to the induction of proliferation, migration, invasiveness, and survival of tumor cells [10,11,44]. The literature also showed that TGF-β plays a role in epithelial ovarian cancer progression by overexpression in the tumor tissue and peritoneal fluid of patients with ovarian cancer [45].

Wang et al. (2014) evaluated TGF-β2 gene expression after an

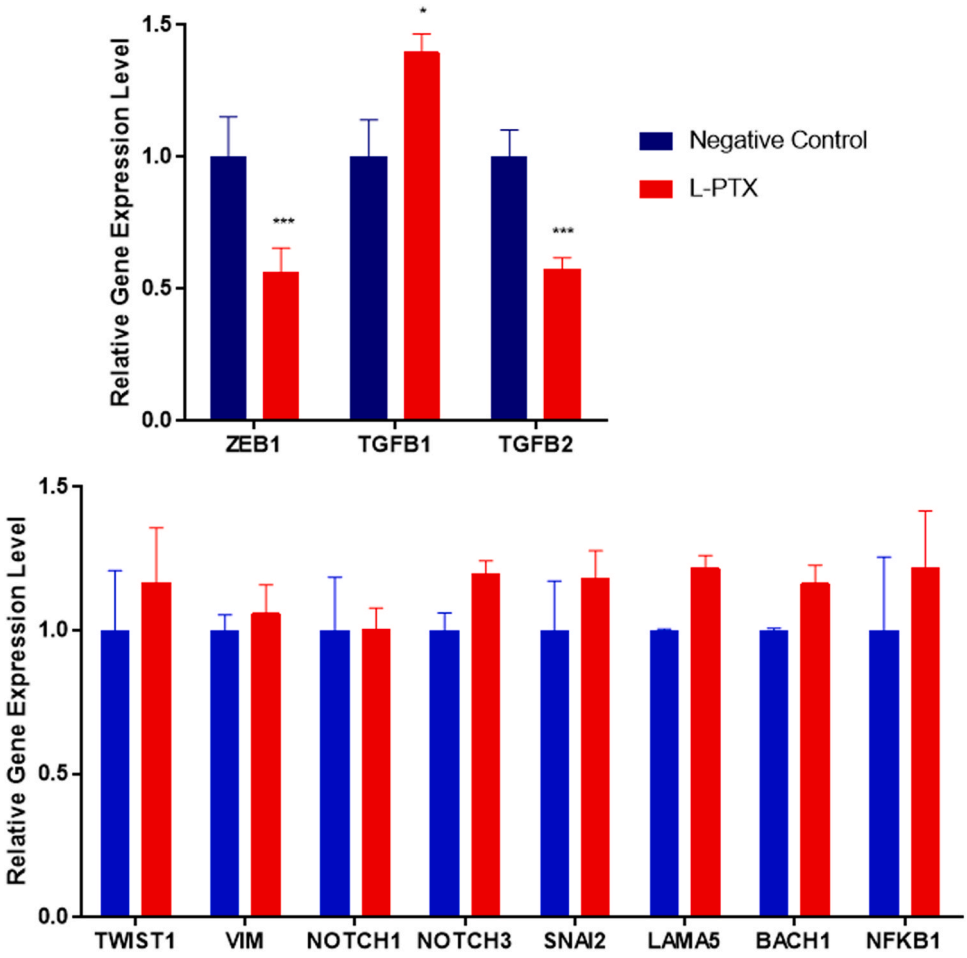

Fig. 6. : qRT-PCR analysis of relative gene expression in A2780 cells without treatment and post treatment with L-PTX. The data were normalized by the ΔΔCt method, using b-actin as housekeeping. Data are presented as mean ± SD. Each sample was measured three times in three independent experiments (n = 3).

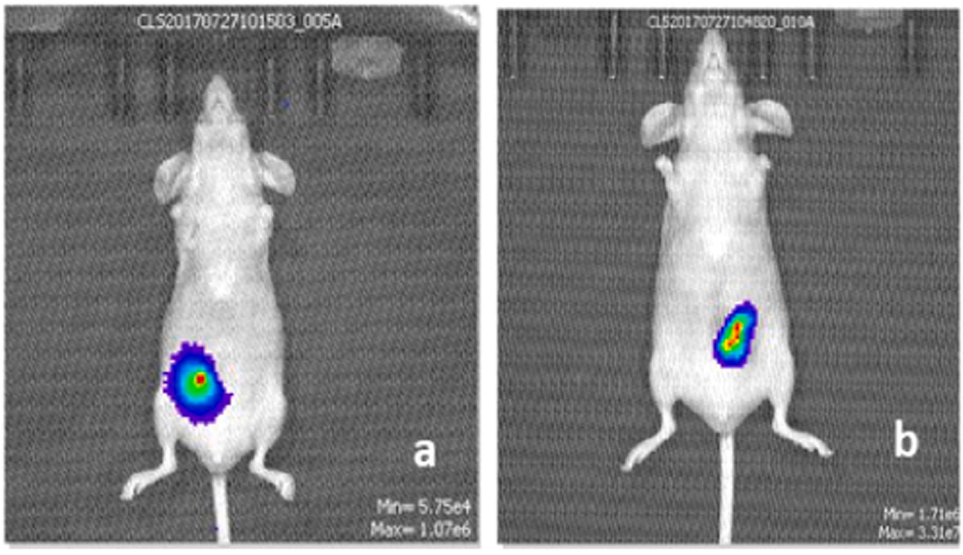

Fig. 7. : Images of two of the five animals three weeks after receiving an A2780-Luc tumor cell injection. Bioluminescence of A2780-Luc cells in animals (a-b), indicated the development of peritoneal ovarian carcinomatosis.

increase in the amount of proteinase PCSK6 in the KGN cell line (ovarian tumor line). This proteinase has a fundamental role in promoting the progression of some tumors to a more aggressive stage, including ovarian cancer. In addition, the authors also hypothesised that the decrease in the TGF-β2 could be related to the promotion of apoptosis [46]. Liu et al. (2015) observed that the increase in the proliferation and

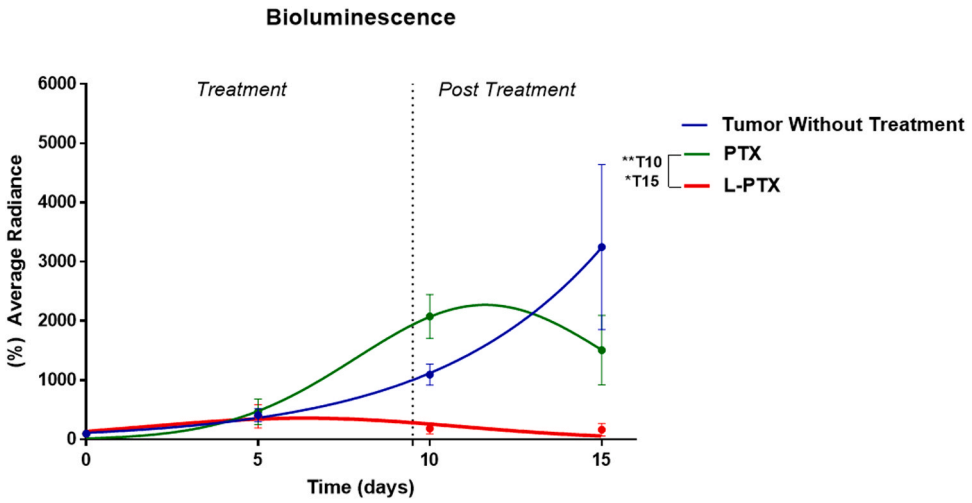

Fig. 8. : Bioluminescence analysis of viable A2780-Luc cells in BALB/c nude mice with ovarian peritoneal carcinomatosis. Five animals per group were treated with the free paclitaxel (PTX) drug or liposomal paclitaxel (L-PTX). Data are presented as a percentage of radiance average over time and normalized with the first measurement. The statistical difference is represented (* $p < 0.05$, ** $p < 0.01$; T10 = 10 days after treatment initiation, T15 = 15 days after treatment initiation).

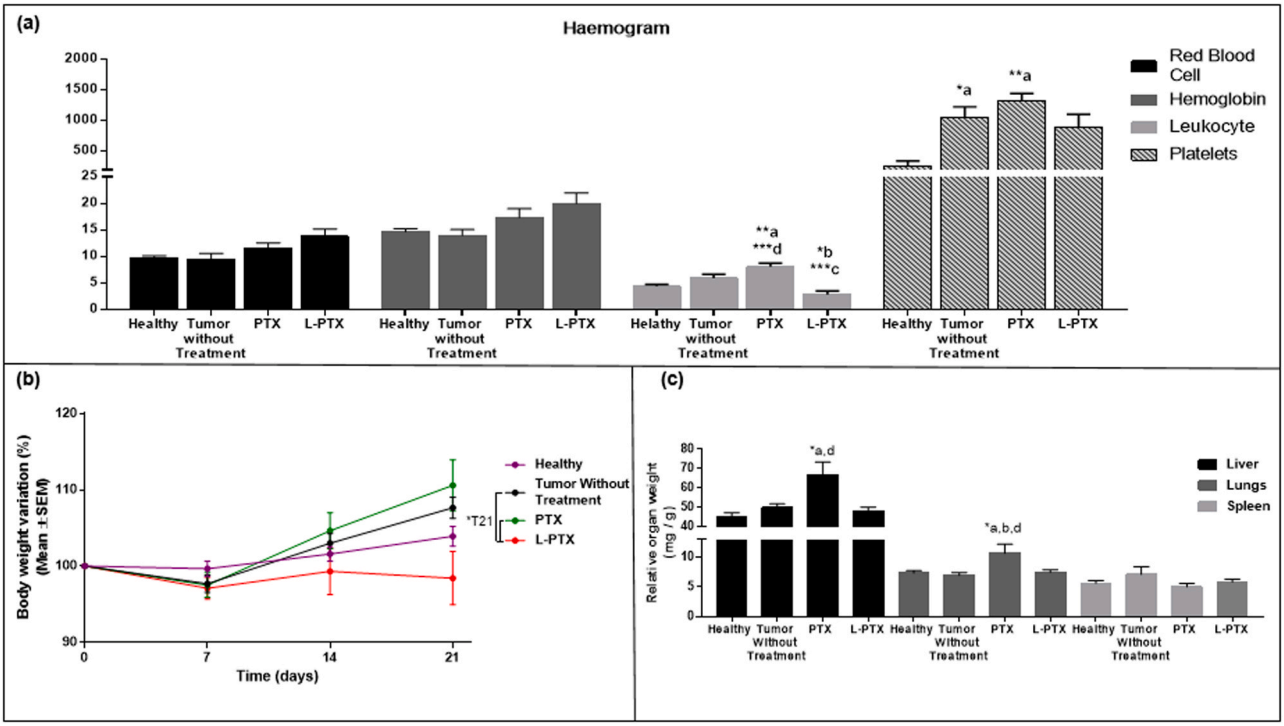

Fig. 9. : Decrease of toxicity evaluated by: (a) hemogram, (b) body weight and (c) relative organ weight of BALB/c nude mice with ovarian peritoneal carcinomatosis 45 days after treatment with L-PTX or PTX. Statistical difference is represented (a = difference with Healthy; b = difference with Tumor Without Treatment; c = difference with PTX; d = difference with L-PTX; T21 = 21 days after treatment initiation; * $p < 0.05$, ** $p < 0.01$, *** $p < 0.001$).

tumor growth of ovarian cancer in nude mice is associated with increased TGF-β2 expression. Particularly in ovarian cancer, TGF-β2 contributes to tumor progression as it is involved in EMT by promoting the loss of cell-cell contact and stimulating both migration and invasion [47].

However, it is important to note that, in a tumor, TGF-β is produced and excreted by mesenchymal cells present in the tumor stroma. Thus, the expression of TGF-β1 and TGF-β2 by untreated tumor cells may show autocrine and paracrine signals. If so, it is plausible to believe that the decrease in ZEB1 can result from the decrease in TGF-β2, since ZEB1 is one of the transcription factors activated by TGF-β-mediated signaling. Likewise, the increase in TGF-β1 could increase ZEB1, but this was not observed, probably because ovarian epithelial tumor cells may lose their ability to respond to signals induced by TGF-β1 [48].

Yeung and colleagues showed that TGF-β1 is an important inhibitor of epithelial cell growth on the normal ovarian surface and has limited effects on ovarian cancer cells, indicating that its role in tumor growth is dependent on genetic mutations in tumor cells and of the tumor microenvironment [48]. Therefore, the increase in TGF-β1 observed in this study is not related to the migratory activity previously seen in the analysis of 2D and 3D migration. EMT is also characterized by increased expression of CDH1 transcriptional repressors, such as ZEB1 and ZEB2, and a consequent increase in mesenchymal cell marker expression, including CDH2 and vimentin [9]. In the results presented in the present

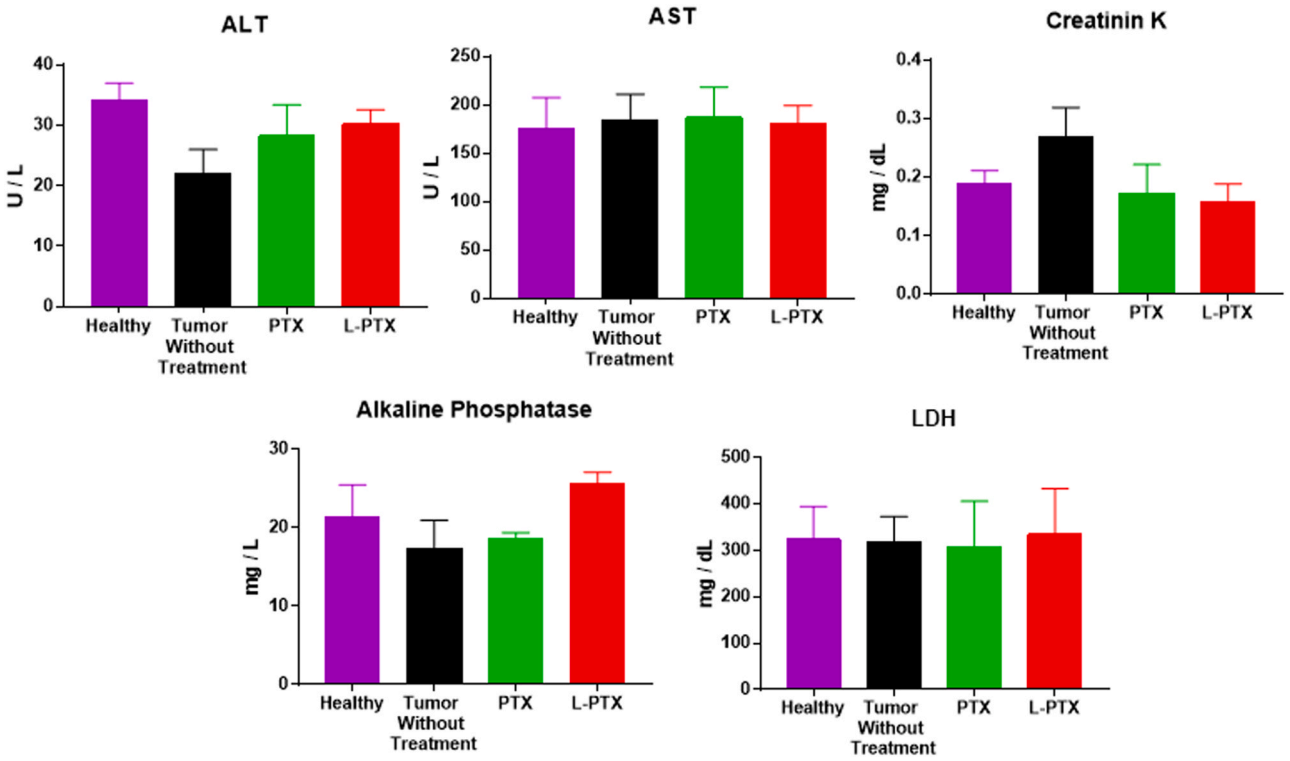

Fig. 10. : Concentrations of ALT, AST, Creatinine K, Alkaline Phosphatase and LDH in peripheral blood of five animals per group treated with the free paclitaxel (PTX) drug or liposomal paclitaxel (L-PTX).

Table 2
Percentage of leukocyte lineage differentiation: lymphocytes, monocytes, basophils, eosinophils and neutrophils. Significant statistical difference: $p \leq 0.05$; $n = 5$ animals per group. Percentage data and standard deviation.

Group	Leukocytes (%)		
	Lymphocytes	Monocytes Basophils Eosinophils	Neutrophils
Animals without tumor	61.9 ± 4.5***c	34.6 ± 2.5***c	6.6 ± 2.7
Animals with tumor and without treatment	45.2 ± 12.4**c	50.9 ± 12.9**c	4.7 ± 1.6
PTX-treated animals with tumor	20.5 ± 10.3	77.0 ± 10.7	3.6 ± 1.0
L-PTX-treated animals with tumor	42.7 ± 8.0*c	53.0 ± 9.2*c	2.7 ± 1.1

The data are expressed as mean ± standard deviation. (*) indicates significant differences detected between the PTX group: * $p < 0.05$, ** $p < 0.01$ and *** $p < 0.001$.

study, there was negative regulation of the transcriptional repressor ZEB 1. According to Chen et al. (2013), the decrease in ZEB1expression is associated with the reduction of colony forming capacity and cell migration in the ovarian cancer cell line, witnessed by researchers for the SKOV-3 and H08910 lines [49]. Likewise, Sakata et al. (2017), when evaluating whether silencing ZEB1 would lead to a reversal of metastatic potential and reversion of chemoresistance, showed that silencing ZEB1 significantly decreased the migration and invasion of PTX-sensitive and PTX-resistant cells [50].

Therefore, it can be inferred that the decrease in colony forming capacity and migration of the A2780 cell line observed in this study may be related to the negative regulation of ZEB1 promoted by the decrease in TGF-β2. However, it must be considered that the transcription factor ZEB1 is a repressor of E-cadherin gene expression [51,52], essential for the acquisition of the mesenchymal phenotype. Thus, it was expected that the decrease in ZEB1 would reflect an increase in the expression of CDH1, an E-cadherin gene, and a decrease in the CDH2 gene, which encodes N-cadherin, a mesenchymal cell protein. However, this was not observed. It is probable that the decrease in cell migration induced by PTX in the liposomal system observed in this study may also be due to other factors, such as the interaction of PTX with microtubules.

Another important process in regulating cell migration is the interaction in microtubule dynamics, present in the cell cytoskeleton [53,54]. The main structural component of microtubules is tubulin, a globular GTP-binding protein found in all eukaryotic cells (classified in the α, β, γ, δ and ε families). It is known that microtubule-stabilizing molecules, such as PTX, inhibit cell migration by binding to β-tubulin in the microtubule lumen [55,56]. Therefore, the entire migration process requires the microtubules to function correctly and PTX may also have been targeted by the inhibition of cell migration to β-tubulin.

In line with the in vitro results, L-PTX also inhibited tumor cell proliferation in ovarian peritoneal carcinomatosis after 4 doses of intravenous treatment, indicating an increase in antitumor activity using the L-PTX formulation when compared to the PTX treatment (Fig. 8). In this case, it is important to note that the use of a nanocarrier was crucial for administration and was also effective in controlling the progression of PTX cell proliferation in the intravenous treatment of peritoneal ovarian carcinomatosis. According to Khalifa et al. (2019), using a nanocarrier to deliver PTX represents a much more effective treatment than free drug use in the bloodstream. The nanocarrier can efficiently direct the delivery of PTX, improve dispersibility due to hydrophobicity, improve its pharmacokinetic profile, avoid rapid excretion when using systemic administration, reduce systemic toxicity, and increase drug accumulation in the tumor [57]. As shown by De Clercq (2019), when gelatin-based microspheres were used as a carrier for the delivery of PTX. In this work, there was efficient targeting and secretion of PTX in the tumor microenvironment, prolonging the effect of chemotherapy while reducing its toxic effects [58]. In the study by Simón-Gracia (2016) with pH-sensitive PTX-loaded POEGMA-PDPA polymersomes, using intraperitoneal administration in disseminated gastric carcinoma, greater antitumor efficacy was observed, being

obtained by targeting and specific penetration into peritoneal tumors. The study indicated that the use of a drug carrier was essential for improving the therapeutic index for PTX [59].

It is known that the combined action of several signaling pathways is responsible for initiating the EMT process [60,61]. EMT regulators have become attractive targets for the development of anti-metastatic therapies, causing impaired cellular motility and consequently migration and invasion. Therefore, we can infer that the liposome is probably accumulating inside the cells and promoting more effective PTX delivery, responsible not only for the antiproliferative and antitumor activity, but also for the inhibition of migratory activity after the drug is removed.

Lee et al. (2007) studied the effects of a solid lipid nanoparticle containing PTX (TM SLN) compared to Taxol®, a clinically approved drug, in treating OVCAR-3 and MCF-7 cells (ovarian and breast cancer, respectively). It was observed that the formulation of TM SLN results in a slow and sustained release of the encapsulated drug, because TM SLN and Taxol® presented similar cytotoxicity, however, only 25% of the encapsulated PTX showed cytotoxic activity within the 24 h analyzed. It is important to note that the authors stated that 75% of the PTX that was encapsulated was not released within those 24 h. Lee emphasizes that it is necessary to evaluate this controlled release in other tests, in addition to elucidating the mechanisms involved [62].

It is noteworthy that PTX carried by the liposome not only improved antiproliferative and anti-migratory actions but was also less toxic than free PTX. The small variation in body weight compared to healthy animals, together with the comparison between organ weight and hematotoxicity analysis, showed that treatment with L-PTX showed results closer to those found in healthy animals. Free PTX was more toxic than L-PTX as it led to an increase in liver/lung weights and increased leukocyte and platelet counts, very similar to the results found in the group with the untreated tumor (Fig. 9).

Assessment of the immune system response to the tumor may play a role in disease progression or suppression. Leukocytes are used as hematological prognostic markers in several types of tumor [63] (Table 2). Many studies have shown that lymphocytes help prevent ovarian cancer development [64,65]. Therefore, a decrease in the number of lymphocytes, lymphocytopenia, due to drug toxicity in the blood results in a reduction of lymphocytes in the tumor region, indicating a weak antitumor immune response [66]. In addition, the neutrophil/lymphocyte ratio can be used as a systemic inflammation response index. The decrease in lymphocytes leads to an increase in the ratio, representing a poor prognosis and low treatment potential [63,67]. On the other hand, monocytes, basophils, and eosinophils are related to cytokine production, associated with excessive cell proliferation, angiogenesis of the tumor region, and metastasis of tumor cells, which contribute to a poor prognosis [68–70].

The toxic effects caused by chemotherapy, both during and after treatment, are a limiting factor that significantly affect the patient's quality of life [37]. Studies demonstrate that using a drug nanocarrier can protect the body from the drug, thus avoiding systemic toxic effects [21], as observed here when using the L-PTX delivery system. These results can be attributed to delivering a high concentration of PTX to tumor cells with much-improved efficacy and a reduced systemic toxicity profile compared to PTX.

Other studies have also investigated the incorporation of PTX in several types of nanocarriers to improve its pharmacokinetic profile and delivery to tumor cells [71–74]. Kim and Park (2017) developed a Paclitaxel-loaded hyaluronan solid nanoemulsion (PTX-HSN) and evaluated the PTX delivery, antitumor activity and possible toxic effects. In vivo toxicity and antitumor activity studies indicated that treatment with PTX-HSN suppressed tumor growth by accumulating drugs in the tumor region. However, the study did not rule out that the amounts of the drug found in other organs (blood, liver, kidneys and lungs) could result in systemic toxicity [75]. The main objective of the study by Yin and collaborators (2016) was to avoid toxicity and optimize the pharmacokinetic behavior and biodistribution of PTX using a formulation with albumin with a polyethylene glycol polymer, PTX-PEG-HSA. This study by Yin et al. (2016) demonstrated that PTX-PEG-HSA was able to circumvent possible toxicities of PTX therapy, compared to the commercial formulations Abraxane™ and Taxol®, by promoting antitumor efficacy improvement and administration security [76].

Ovarian cancer metastasis is the main concern of ovarian cancer and is an indicator of poor prognosis. The results of this study showed that the use of liposomal PTX leads to more effective control of tumor cell proliferation both in vitro and in vivo, in addition to inhibiting migration and not inducing systemic toxicity.

5. Conclusion

The data obtained in this study corroborated that using a nanocarrier to deliver paclitaxel improves the antitumor action of this drug. The liposomal PTX improved cytotoxic activity against tumor cells, decreasing the IC_{50} value compared to free PTX. A marked antimigratory response promoted by the decrease in TGF-β2 and ZEB1 was also observed. Inhibition of A2780 cell proliferation in the abdominal region of the animal was observed, together with the decreased adverse effects of chemotherapy, compared to the use of non-encapsulated PTX. Collectively, the results of this liposomal encapsulated paclitaxel nanosystem showed that this formulation potentially represents a more effective treatment strategy than the free drug, warranting further investigation for the treatment of metastatic ovarian cancer.

CRediT authorship contribution statement

Raquel Santos Faria: in vitro and in vivo collection, data analysis and interpretation and drafting of the manuscript. Luiza Ianny de Lima: in vivo collection, data analysis and interpretation. Raphael Severino Bonadio: collection, analysis and interpretation of gene expression data. João Paulo Figueiró Longo: experimental design/development, in vitro/in vivo data analysis and interpretation. Marjorie Coimbra: provision of the specific liposome formulation and characterization, manuscript drafting and critical revision. João Nunes: experimental design/development and critical revision of the manuscript. Sergio Moya: experimental design and critical revision of the manuscript. Mônica Cristina de Oliveira: provision of the specific liposome formulation/characterization, manuscript drafting and critical revision. Ricardo Bentes de Azevedo: experimental design/development, manuscript drafting and critical revision, and final approval of the article submitted for publication. All authors read and approved the final version of the manuscript submitted for publication.

Conflict of interest statement

We declare that we have no financial and personal relationships with other people or organizations that can inappropriately influence our work, there is no professional or other personal interest of any nature or kind in any product, service and/or company that could be construed as influencing the position presented in, or the review of, this manuscript.

Acknowledgments

This work was supported by: CNPq, CAPES and FAP-DF.

References

[1] T.S. Lawrence, S.A. Rosenberg, R.A. DePinho, R.A. Weinberg, Cancer: Principles & Practice of Oncology, Lippincott Williams & Wilkins, 2011.
[2] J. Ferlay, M. Colombet, I. Soerjomataram, C. Mathers, D.M. Parkin, M. Piñeros, A. Znaor, F. Bray, Estimating the global cancer incidence and mortality in 2018: GLOBOCAN sources and methods, Int. J. Cancer 144 (2019) 1941–1953.

[3] C.-M. Ho, S.-F. Chang, C.-C. Hsiao, T.-Y. Chien, D.T.-B. Shih, Isolation and characterization of stromal progenitor cells from ascites of patients with epithelial ovarian adenocarcinoma, J. Biomed. Sci. 19 (2012) 1–10.

[4] S. Banerjee, S.B. Kaye, New strategies in the treatment of ovarian cancer: current clinical perspectives and future potential, Clin. Cancer Res. 19 (2013) 961–968.

[5] C.P. Bracken, P.A. Gregory, N. Kolesnikoff, A.G. Bert, J. Wang, M.F. Shannon, G. J. Goodall, A double-negative feedback loop between ZEB1-SIP1 and the microRNA-200 family regulates epithelial-mesenchymal transition, Cancer Res. 68 (2008) 7846–7854.

[6] U. Wellner, J. Schubert, U.C. Burk, O. Schmalhofer, F. Zhu, A. Sonntag, B. Waldvogel, C. Vannier, D. Darling, A. Zur Hausen, The EMT-activator ZEB1 promotes tumorigenicity by repressing stemness-inhibiting microRNAs, Nat. Cell Biol. 11 (2009) 1487–1495.

[7] J. Dou, N. Gu, Emerging strategies for the identification and targeting of cancer stem cells, Tumor Biol. 31 (2010) 243–253.

[8] M.A. Nieto, Epithelial plasticity: a common theme in embryonic and cancer cells, Science 342 (2013), 1234850.

[9] D. Kong, Y. Li, Z. Wang, F.H. Sarkar, Cancer stem cells and epithelial-to-mesenchymal transition (EMT)-phenotypic cells: are they cousins or twins? Cancers (Basel) 3 (2011) 716–729.

[10] J. Massagué, TGF$β$ signalling in context, Nat. Rev. Mol. Cell Biol. 13 (2012) 616–630.

[11] N. Hagimoto, K. Kuwano, I. Inoshima, M. Yoshimi, N. Nakamura, M. Fujita, T. Maeyama, N. Hara, TGF-β1 as an enhancer of Fas-mediated apoptosis of lung epithelial cells, J. Immunol. 168 (2002) 6470–6478.

[12] S.A. Mani, W. Guo, M.-J. Liao, E.N. Eaton, A. Ayyanan, A.Y. Zhou, M. Brooks, F. Reinhard, C.C. Zhang, M. Shipitsin, The epithelial-mesenchymal transition generates cells with properties of stem cells, Cell 133 (2008) 704–715.

[13] J.P. Thiery, H. Acloque, R.Y.J. Huang, M.A. Nieto, Epithelial-mesenchymal transitions in development and disease, Cell 139 (2009) 871–890.

[14] X. He, J. Wang, F. Zhao, F. Yu, D. Chen, K. Cai, C. Yang, J. Chen, J. Dou, Antitumor efficacy of viable tumor vaccine modified by heterogenetic ESAT-6 antigen and cytokine IL-21 in melanomatous mouse, Immunol. Res. 52 (2012) 240–249.

[15] A.N. Gordon, C.O. Granai, P.G. Rose, J. Hainsworth, A. Lopez, C. Weissman, R. Rosales, T. Sharpington, Phase II study of liposomal doxorubicin in platinum- and paclitaxel-refractory epithelial ovarian cancer, J. Clin. Oncol. 18 (2000) 3093–3100.

[16] S.M. Campos, R.T. Penson, A.R. Mays, R.S. Berkowitz, A.F. Fuller, A. Goodman, U. A. Matulonis, A. Muzikansky, M.V. Seiden, The clinical utility of liposomal doxorubicin in recurrent ovarian cancer, Gynecol. Oncol. 81 (2001) 206–212.

[17] K. Iizuka, C. Jin, K. Eshima, M.H. Hong, K. Eshima, M. Fukushima, Anticancer activity of the intraperitoneal-delivered DFP-10825, the cationic liposome-conjugated RNAi molecule targeting thymidylate synthase, on peritoneal disseminated ovarian cancer xenograft model, Drug Des. Dev. Ther. 12 (2018) 673–683.

[18] A.J. ten Tije, J. Verweij, W.J. Loos, A. Sparreboom, Pharmacological effects of formulation vehicles: implications for cancer chemotherapy, Clin. Pharm. 42 (2003) 665–685.

[19] L.M. Zasadil, K.A. Andersen, D. Yeum, G.B. Rocque, L.G. Wilke, A.J. Tevaarwerk, R. T. Raines, M.E. Burkard, B.A. Weaver, Cytotoxicity of paclitaxel in breast cancer is due to chromosome missegregation on multipolar spindles, Sci. Transl. Med. 6 (2014) 229, 229ra43-229ra43.

[20] F.E. Walker, Paclitaxel (TAXOL®): side effects and patient education issues, in: Proceedings of the Seminars in oncology nursing, Vol. 9, Elsevier, 1993, pp. 6–10.

[21] S. Friberg, A.M. Nyström, NANOMEDICINE: will it offer possibilities to overcome multiple drug resistance in cancer? J. Nanobiotechnol. 14 (2016) 1–17, https://doi.org/10.1186/s12951-016-0172-2.

[22] Dúran, N. Nanotecnologia: introdução, preparação e caracterização de nanomateriais e exemplos de aplicação; Artliber, 2006; ISBN 8588098334.

[23] G. Caracciolo, S. Palchetti, L. Digiacomo, R.Z. Chiozzi, A.L. Capriotti, H. Amenitsch, P.M. Tentori, V. Palmieri, M. Papi, F. Cardarelli, Human biomolecular corona of liposomal doxorubicin: the overlooked factor in anticancer drug delivery, ACS Appl. Mater. Interfaces 10 (2018) 22951–22962.

[24] S. Bhowmik, S. Bhowmick, K. Maiti, A. Chakra, P. Shahi, D. Jain, T. Rajamannar, Two multicenter Phase I randomized trials to compare the bioequivalence and safety of a generic doxorubicin hydrochloride liposome injection with Doxil® or Caelyx® in advanced ovarian cancer, Cancer Chemother. Pharmacol. 82 (2018) 521–532, https://doi.org/10.1007/s00280-018-3643-3.

[25] Z. Tang, W. Feng, Y. Yang, Q. Wang, Gemcitabine-loaded RGD modified liposome for ovarian cancer: preparation, characterization and pharmacodynamic studies, Drug Des. Devel. Ther. 13 (2019) 3281–3290.

[26] A.C. Khayrani, H. Mahmud, A. Oo, M.H. Zahra, M. Oze, J. Du, M.J. Alam, S. M. Afify, H. Quora, T. Shigehiro, A.S. Calle, N. Okada, A. Seno, K. Fujita, H. Hamada, Y. Seno, T. Mandai, M. Seno, Targeting ovarian cancer cells overexpressing CD44 with immunoliposomes encapsulating glycosylated paclitaxel, Int. J. Mol. Sci. 20 (2019) 1042, https://doi.org/10.3390/ijms20051042.

[27] M.V. Barbosa, L.O.F. Monteiro, A.R. Malagutti, M.C. Oliveira, A.D. Carvalho-Junior, E.A. Leite, Comparative study of first-derivative spectrophotometry and high performance liquid chromatography methods for quantification of paclitaxel in liposomal formulation, J. Braz. Chem. Soc. 26 (2015) 1338–1343.

[28] D. dos Santos Ferreira, S.D. Faria, S.C. de Araújo Lopes, C.S. Teixeira, A. Malachias, R. Magalhães-Paniago, J.D. de Souza Filho, B.L. Oliveira, J.P. de, A.R. Guimarães, P. Caravan, Development of a bone-targeted pH-sensitive liposomal formulation containing doxorubicin: physicochemical characterization, cytotoxicity, and biodistribution evaluation in a mouse model of bone metastasis, IJN 11 (2016) 3737–3751.

[29] C.D. Gamarra-Luques, A.A. Goyeneche, M.B. Hapon, C.M. Telleria, Mifepristone prevents repopulation of ovarian cancer cells escaping cisplatin-paclitaxel therapy, BMC Cancer 12 (2012) 1–16.

[30] M.S. Franco, M.C. Roque, M.C. Oliveira, Short and long-term effects of the exposure of breast cancer cell lines to different ratios of free or co-encapsulated liposomal paclitaxel and doxorubicin, Pharmaceutics 11 (2019) *11*, https://doi.org/10.3390/pharmaceutics11040178.

[31] J.M. Coelho, N.S. Camargo, R. Ganassin, M.C.O. Rocha, C. Merker, J. Böttner, I. Estrela-Lopis, K.R. Py-Daniel, K.V. Jardim, M.H. Sousa, Oily core/amphiphilic polymer shell nanocapsules change the intracellular fate of doxorubicin in breast cancer cells, J. Mater. Chem. B 7 (2019) 6390–6398.

[32] A.L. dos Santos Câmara, G. Nagel, H.R. Tschiche, C.M. Cardador, L.A. Muehlmann, D.M. de Oliveira, P.Q. Alvim, R.B. Azevedo, M. Calderón, J.P. Figueiro Longo, Acid-sensitive lipidated doxorubicin prodrug entrapped in nanoemulsion impairs lung tumor metastasis in a breast cancer model, Nanomedicine 12 (2017) 1751–1765.

[33] R. Ganassin, C. Merker, M.C. Rodrigues, N.F. Guimarães, C.S.C. Sodré, Q. Ferreira, S. da, S.W. da Silva, A.S. Ombredane, G.A. Joanitti, K.R. Py-Daniel, Nanocapsules for the co-delivery of selol and doxorubicin to breast adenocarcinoma 4T1 cells in vitro, Artif. Cells, Nanomed., Biotechnol. 46 (2018) 2002–2012.

[34] R.A. Weinberg, The biology of cancer, Garland science, 2013.

[35] M.D. Goodman, S. McPartland, D. Detelich, M.W. Saif, Chemotherapy for intraperitoneal use: a review of hyperthermic intraperitoneal chemotherapy and early post-operative intraperitoneal chemotherapy, J. Gastrointest. Oncol. 7 (2016) 45–57.

[36] W.J. Gradishar, D. Krasnojon, S. Cheporov, A.N. Makhson, G.M. Manikhas, A. Clawson, P. Bhar, J.R. McGuire, J. Iglesias, Phase II trial of nab-paclitaxel compared with docetaxel as first-line chemotherapy in patients with metastatic breast cancer: final analysis of overall survival, Clin. Breast Cancer 12 (2012) 313–321.

[37] M.S. Franco, M.C. Roque, A.L.B. de Barros, J. de Oliveira Silva, G.D. Cassali, M. C. Oliveira, Investigation of the antitumor activity and toxicity of long-circulating and fusogenic liposomes co-encapsulating paclitaxel and doxorubicin in a murine breast cancer animal model, Biomed. Pharmacother. 109 (2019) 1728–1739.

[38] K. Pardali, A. Moustakas, Actions of TGF-$β$ as tumor suppressor and pro-metastatic factor in human cancer, Biochim. Biophys. Acta (BBA)-Rev. Cancer 1775 (2007) 21–62.

[39] M. Gao, Y. Xu, L. Qiu, Enhanced combination therapy effect on paclitaxel-resistant carcinoma by chloroquine co-delivery via liposomes, Int. J. Nanomed. 10 (2015) 6615–6632, https://doi.org/10.2147/IJN.S91463.

[40] C. Ricciardelli, N.A. Lokman, S. Cheruvu, I.A. Tan, M.P. Ween, C.E. Pyragius, M. K. Oehler, C. Ricciardelli, N.A. Lokman, S. Cheruvu, I.A. Tan, M.P. Ween, C. E. Pyragius, A. Ruszkiewicz, P. Hoffmann, M.K. Oehler, Transketolase is upregulated in metastatic peritoneal implants and promotes ovarian cancer cell proliferation, Clin. Exp. Metastas-.-. 32 (5) (2015) 441–455, https://doi.org/10.1007/s10585-015-9718-1.

[41] R. Derynck, R.J. Akhurst, Differentiation plasticity regulated by TGF-$β$ family proteins in development and disease, Nat. Cell Biol. 9 (2007) 1000–1004.

[42] B.P. Muthusamy, E.H. Budi, Y. Katsuno, M.K. Lee, S.M. Smith, A.M. Mirza, R. J. Akhurst, R. Derynck, ShcA protects against epithelial-mesenchymal transition through compartmentalized inhibition of tgf-β-induced smad activation, PLoS Biol. 13 (2015), 1002325.

[43] E.-J. Tan, A.-K. Olsson, A. Moustakas, Reprogramming during epithelial to mesenchymal transition under the control of TGFβ, Cell Adh. Migr. 9 (2015) 233–246.

[44] S.P. Fink, S.E. Swinler, J.D. Lutterbaugh, J. Massagué, S. Thiagalingam, K. W. Kinzler, B. Vogelstein, J.K.V. Willson, S. Markowitz, Transforming growth factor-β-induced growth inhibition in a Smad4 mutant colon adenoma cell line, Cancer Res. 61 (2001) 256–260.

[45] L.D. Dunfield, M.W. Nachtigal, Inhibition of the antiproliferative effect of TGF β by EGF in primary human ovarian cancer cells, Oncogene 22 (2003) 4745–4751.

[46] Y. Wang, J. Zhou, L. Qiu, X. Wang, L. Chen, T. Liu, W. Di, Cisplatin–alginate conjugate liposomes for targeted delivery to EGFR-positive ovarian cancer cells, Biomaterials 35 (2014) 4297–4309.

[47] T.-V. Do, L.A. Kubba, H. Du, C.D. Sturgis, T.K. Woodruff, Transforming growth factor-$β$1, transforming growth factor-$β$2, and transforming growth factor-$β$3 enhance ovarian cancer metastatic potential by inducing a Smad3-dependent epithelial-to-mesenchymal transition, Mol. Cancer Res. 6 (2008) 695–705.

[48] T.-L. Yeung, C.S. Leung, K.-K. Wong, G. Samimi, M.S. Thompson, J. Liu, T.M. Zaid, S. Ghosh, M.J. Birrer, S.C. Mok, TGF-β modulates ovarian cancer invasion by upregulating CAF-derived versican in the tumor microenvironment, Cancer Res 73 (2013) 5016–5028.

[49] D. Chen, J. Wang, Y. Zhang, J. Chen, C. Yang, W. Cao, H. Zhang, Y. Liu, J. Dou, Effect of down-regulated transcriptional repressor ZEB1 on the epithelial-mesenchymal transition of ovarian cancer cells, Int. J. Gynecol. Cancer 23 (2013) 1357–1366.

[50] J. Sakata, F. Utsumi, S. Suzuki, K. Niimi, E. Yamamoto, K. Shibata, T. Senga, F. Kikkawa, H. Kajiyama, Inhibition of ZEB1 leads to inversion of metastatic characteristics and restoration of paclitaxel sensitivity of chronic chemoresistant ovarian carcinoma cells, Oncotarget 8 (2017) 99482–99494.

[51] S. Prislei, E. Martinelli, G.F. Zannoni, M. Petrillo, F. Filippetti, M. Mariani, S. Mozzetti, G. Raspaglio, G. Scambia, C. Ferlini, Role and prognostic significance of the epithelial-mesenchymal transition factor ZEB2 in ovarian cancer, Oncotarget 6 (2015) 18966–18979.

[52] S.-M. Park, A.B. Gaur, E. Lengyel, M.E. Peter, The miR-200 family determines the epithelial phenotype of cancer cells by targeting the E-cadherin repressors ZEB1 and ZEB2, Genes Dev. 22 (2008) 894–907.
[53] E. Komlodi-Pasztor, D. Sackett, J. Wilkerson, T. Fojo, Mitosis is not a key target of microtubule agents in patient tumors, Nat. Rev. Clin. Oncol. 8 (2011) 244–250.
[54] V. Čermák, V. Dostál, M. Jelínek, L. Libusová, J. Kovář, D. Rösel, J. Brábek, Microtubule-targeting agents and their impact on cancer treatment, Eur. J. Cell Biol. 99 (2020), 151075.
[55] B.P. Bouchet, A. Akhmanova, Microtubules in 3D cell motility, J. Cell Sci. 130 (2017) 39–50.
[56] J.J. Field, P.T. Northcote, I. Paterson, K.-H. Altmann, J.F. Díaz, J.H. Miller, Zampanolide, a microtubule-stabilizing agent, is active in resistant cancer cells and inhibits cell migration, IJMS 18 (2017) 971.
[57] A.M. Khalifa, M.A. Elsheikh, A.M. Khalifa, Y.S.R. Elnaggar, Current strategies for different paclitaxel-loaded Nano-delivery Systems towards therapeutic applications for ovarian carcinoma: a review article, J. Control. Release 311 (2019) 125–137.
[58] K. De Clercq, F. Xie, O. De Wever, B. Descamps, A. Hoorens, A. Vermeulen, W. Ceelen, C. Vervaet, Preclinical evaluation of local prolonged release of paclitaxel from gelatin microspheres for the prevention of recurrence of peritoneal carcinomatosis in advanced ovarian cancer, Sci. Rep. 9 (2019) 1–19, https://doi.org/10.1038/s41598-019-51419-y.
[59] L. Simón-Gracia, H. Hunt, P.D. Scodeller, J. Gaitzsch, G.B. Braun, A.M.A. Willmore, E. Ruoslahti, G. Battaglia, T. Teesalu, Paclitaxel-loaded polymersomes for enhanced intraperitoneal chemotherapy, Mol. Cancer Ther. 15 (2016) 670–679, https://doi.org/10.1158/1535-7163.MCT-15-0713-T.
[60] E. Colas, N. Pedrola, L. Devis, T. Ertekin, I. Campoy, E. Martínez, M. Llauradó, M. Rigau, M. Olivan, M. Garcia, The EMT signaling pathways in endometrial carcinoma, Clin. Transl. Oncol. 14 (2012) 715–720.
[61] M. Teeuwssen, R. Fodde, Wnt signaling in ovarian cancer stemness, EMT, and therapy resistance, J. Clin. Med. 8 (2019) 1658.
[62] M.-K. Lee, S.-J. Lim, C.-K. Kim, Preparation, characterization and in vitro cytotoxicity of paclitaxel-loaded sterically stabilized solid lipid nanoparticles, Biomaterials 28 (2007) 2137–2146.
[63] H. Zhang, Q. Huo, L. Huang, Y. Cheng, Y. Liu, H. Bao, Genotoxicity and subchronic toxicological study of a novel ginsenoside derivative 25-OCH3-PPD in beagle dogs, J. Ginseng Res. 43 (2019) 562–571.
[64] J. Hamanishi, M. Mandai, M. Iwasaki, T. Okazaki, Y. Tanaka, K. Yamaguchi, T. Higuchi, H. Yagi, K. Takakura, N. Minato, Programmed cell death 1 ligand 1 and tumor-infiltrating CD8+ T lymphocytes are prognostic factors of human ovarian cancer, Proc. Natl. Acad. Sci. 104 (2007) 3360–3365.
[65] K. Abiko, N. Matsumura, J. Hamanishi, N. Horikawa, R. Murakami, K. Yamaguchi, Y. Yoshioka, T. Baba, I. Konishi, M. Mandai, IFN-γ from lymphocytes induces PD-L1 expression and promotes progression of ovarian cancer, Br. J. Cancer 112 (2015) 1501–1509.
[66] M.Q. Yuan, F. Zhu, J.Y. Lou, W.M. Yuan, L. Fu, S. Liu, Z.Z. Zhang, C.Y. Liu, Q. He, The anti-tumoral efficacy of a docetaxel-loaded liposomal drug delivery system modified with transferrin for ovarian cancer, Drug Res 64 (2014) 195–202, https://doi.org/10.1055/s-0033-1355335.
[67] H. Cho, H.W. Hur, S.W. Kim, S.H. Kim, J.H. Kim, Y.T. Kim, K. Lee, Pre-treatment neutrophil to lymphocyte ratio is elevated in epithelial ovarian cancer and predicts survival after treatment, Cancer Immunol. Immunother. 58 (2009) 15–23, https://doi.org/10.1007/s00262-008-0516-3.
[68] H. Ishii, M. Takahara, T. Nagato, L.L. Kis, N. Nagy, K. Kishibe, Y. Harabuchi, E. Klein, Monocytes enhance cell proliferation and LMP1 expression of nasal natural killer/T-cell lymphoma cells by cell contact-dependent interaction through membrane-bound IL-15, Int. J. Cancer 130 (2012) 48–58, https://doi.org/10.1002/ijc.25969.
[69] E.N. Arwert, A.S. Harney, D. Entenberg, Y. Wang, J.W. Pollard, J.S. Condeelis, Abstract B26: identification of molecular and functional differences in tumor-associated macrophage subsets, Cancer Res 73 (2013) B26, https://doi.org/10.1158/1538-7445.TIM2013-B26.
[70] J. Lu, X. Liu, Y.-P. Liao, X. Wang, A. Ahmed, W. Jiang, Y. Ji, H. Meng, A.E. Nel, Breast cancer chemo-immunotherapy through liposomal delivery of an immunogenic cell death stimulus plus interference in the IDO-1 pathway, ACS Nano 12 (2018) 11041–11061, https://doi.org/10.1021/acsnano.8b05189.
[71] W.R. Perkins, I. Ahmad, X. Li, D.J. Hirsh, G.R. Masters, C.J. Fecko, J. Lee, S. Ali, J. Nguyen, J. Schupsky, C. Herbert, A.S. Janoff, E. Mayhew, Novel therapeutic nano-particles (lipocores): trapping poorly water soluble compounds, Int. J. Pharm. 200 (2000) 27–39, https://doi.org/10.1016/S0378-5173(00)00329-X.
[72] Y. Liu, D. Zheng, M. Liu, J. Bai, X. Zhou, B. Gong, J. Lü, Y. Zhang, H. Huang, W. Luo, G. Huang, Downregulation of glypican-3 expression increases migration, invasion, and tumorigenicity of human ovarian cancer cells, Tumor Biol. 36 (2015) 7997–8006, https://doi.org/10.1007/s13277-015-3528-6.
[73] Y.-A. Shen, W.-H. Li, P.-H. Chen, C.-L. He, Y.-H. Chang, C.-M. Chuang, Intraperitoneal delivery of a novel liposome-encapsulated paclitaxel redirects metabolic reprogramming and effectively inhibits cancer stem cells in Taxol (®)-resistant ovarian cancer, Am. J. Transl. Res. 7 (2015) 841–855.
[74] S. Yao, L. Li, X.-T. Su, K. Wang, Z.-J. Lu, C.-Z. Yuan, J.-B. Feng, S. Yan, B.-H. Kong, K. Song, Development and evaluation of novel tumor-targeting paclitaxel-loaded nano-carriers for ovarian cancer treatment: in vitro and in vivo, J. Exp. Clin. Cancer Res. 37 (2018) 29, https://doi.org/10.1186/s13046-018-0700-z.
[75] J.-E. Kim, Y.-J. Park, Paclitaxel-loaded hyaluronan solid nanoemulsions for enhanced treatment efficacy in ovarian cancer, Int. J. Nanomed. 12 (2017) 645–658.
[76] T. Yin, H. Cai, J. Liu, B. Cui, L. Wang, L. Yin, J. Zhou, M. Huo, Biological evaluation of PEG modified nanosuspensions based on human serum albumin for tumor targeted delivery of paclitaxel, Eur. J. Pharm. Sci. 83 (2016) 79–87, https://doi.org/10.1016/j.ejps.2015.12.019.